Cellulose (2021) 28:6983–6993
https://doi.org/10.1007/s10570-021-03996-3

ORIGINAL RESEARCH

Achromatic optical waveplates based on cellulose nanocrystals

Chenxi Li · Nan Wang · Julian Evans · Sailing He

Received: 14 December 2020 / Accepted: 10 June 2021 / Published online: 16 June 2021

Abstract Cellulose nanocrystals (CNCs) derived from native cellulose can self-assemble into liquid crystals (LCs) and preserve the LC alignment in solid films that are attractive for the preparation of optical materials and devices from bottom-up manufacturing. Birefringent aligned CNC films provide the desired phase retardation for a narrow band of wavelengths due to the intrinsic wavelength-dependent birefringence of CNCs. Here, we produce a 1/4 λ achromatic CNC-based waveplate consisting of three layers of birefringent CNC films with phase retardations and slow axis directions, which are calculated by Jones Matrix, with optimized achromatic properties. Three uniform CNC films are prepared by aligning nematic CNC LCs doped with polyethylene glycol on patterned polydimethylsiloxane substrates. The fabricated achromatic waveplate is characterized by measuring the transmission spectra, and its maximum deviation of phase retardation is around 0.06 for the wavelength range of 460–660 nm. The achromatic performance is improved by one order of magnitude compared with the single birefringent CNC films. Our CNC-based achromatic waveplate has good optical homogeneity, flexibility and can be tailored into arbitrary shape.

Chenxi Li and Nan Wang have contributed equally to this manuscript.

Supplementary Information The online version contains supplementary material available at https://doi.org/10.1007/s10570-021-03996-3.

C. Li · N. Wang · J. Evans · S. He
Centre for Optical and Electromagnetic Research, College of Optical Science and Engineering, State Key Laboratory of Modern Optical Instrumentation, Zhejiang University, Hangzhou 310058, China
e-mail: julian.evans@colorado.edu

S. He
e-mail: sailing@zju.edu.cn

N. Wang (✉) · S. He
Ningbo Research Institute, Zhejiang University, Ningbo 315100, China
e-mail: wangnan509@zju.edu.cn

S. He
Department of Electromagnetic Engineering, School of Electrical Engineering, Royal Institute of Technology, 100 44 Stockholm, Sweden

Keywords Cellulose nanocrystals · Waveplates · Achromatism · Liquid crystals · Nematics

Introduction

Cellulose nanocrystals (CNCs) are highly anisotropic rod-shaped nanoparticles and can be obtained by acid hydrolyzing of native cellulose (Yu et al. 2013). CNCs are widely used for material science and engineering applications (Habibi et al. 2010; Jonoobi et al. 2015). CNC-based materials exhibit useful optical properties and good mechanical performance, and are derived from the most abundant biopolymer (Frka-Petesic and Vignolini 2019; Lagerwall et al. 2014; Qu et al. 2019). Since CNCs can be recycled from waste or biomass, such as bacteria (Araki and Kuga 2001), cotton (Ling et al. 2019; Sun et al. 2016), woods (Chen et al. 2015) and so on, it is desirable to expand the applications of CNC-based materials and enhance the sustainability of the cellulose-rich devices (Frka-Petesic and Vignolini 2019). Advanced optical films are fabricated by the self-assembly of CNCs, such as reflecting films (Yao et al. 2017; Zhao et al. 2018) and birefringent films (Cranston and Gray 2008; Kose et al. 2019; Parker et al. 2018). CNC suspensions show well-known liquid crystal (LC) phases above a critical concentration of CNCs (Habibi et al. 2010). CNC films fabricated by evaporating the solvent from the LC phase can capture the orientational ordering (Pan et al. 2010; Tran et al. 2020). Helically ordered CNCs are usually obtained and have been extensively used to produce reflecting films (Beck et al. 2013), and the helical ordering of the CNCs leads to strong Bragg reflection (De La Cruz et al. 2018; Fernandes et al. 2017). Since CNCs self-assembled into ordered structures induce considerable optical birefringence, fabrication of birefringent film by CNCs has also been explored (Haywood et al. 2017; Hoeger et al. 2011; Mendoza-Galván et al. 2019). However, helically ordered CNCs have intrinsic drawbacks for the preparation of high-quality birefringent films, because the LC directors tend to deviate from being uniformly aligned. Therefore, the prepared birefringent films usually suffer from lower optical birefringence.

Recently, we have demonstrated that pH control reliably switches between helical alignment and uniaxial alignment of CNC LCs. pH below $\sim$ 1.5 or above $\sim$ 10 can produce uniaxial nematic alignment due to the reduced Debye length (Li et al. 2019b). Based on this method, we showed the feasibility of producing CNC birefringent films or optical waveplates by nematic phase (Li et al. 2019a).The obtained waveplates have high optical birefringence compared with the previous reports (Mendoza-Galván et al. 2019; Parker et al. 2018). Furthermore, the CNC-based waveplates are flexible, have good processability and can be conveniently made into zeroth-order phase retarder at low cost. However, the optical waveplates demonstrated in our preliminary results are only designed to work at single wavelength, while for a large number of practical applications, such as spectropolarimetry (Abuleil and Abdulhalim 2014), astronomical observance (Roberts et al. 2009) and so on, achromatic waveplates are more desirable. Achromatic waveplates require that the phase retardation induced by the waveplate remains constant for a broad band of wavelengths, and are usually fabricated by combining two anisotropic crystals (such as quartz and magnesium fluoride) which have different dispersion curves (Beckers 1971; Hariharan 1995, 2002; Saha et al. 2012). Unfortunately such achromatic waveplates are generally fragile, difficult to polish and expensive (Jen et al. 2011). Preparing achromatic waveplates with renewable flexible biopolymers such as cellulose is very attractive. Even though it is desirable to prepare achromatic waveplates only by CNC films, how to achieve achromatism remains a problem. It is difficult to directly tailor the birefringence dispersion of the uniaxial nematic CNCs obtained in the experiment.

In this paper, we propose and demonstrate a method to fabricate achromatic waveplates with CNC films. A 1/4 λ achromatic waveplate composed of three uniformly aligned nematic CNC birefringent films that is fabricated based on our recently published method (Li et al. 2019a) is demonstrated. The phase retardation and the direction of slow axis of each CNC film are determined by Jones matrix calculation, and the achromatic properties are optimized. Each CNC film with desired phase retardation is produced by aligning CNC nematic LCs doped with polyethylene glycol (PEG) on patterned polydimethylsiloxane (PDMS) substrates. To determine the required thickness of the CNC films, optical birefringence of the PEG-doped CNC nematic has been measured. Then thickness of each CNC film is well controlled by the

pattern on the PDMS substrates. The orientation of slow axis of each CNC film is experimentally determined and arranged as designed. The obtained CNC-based achromatic waveplate is characterized by measuring the transmission spectra of the waveplate between two polarizers. The fabricated achromatic waveplate is measured to have a maximum deviation of phase retardation of 0.06 for the wavelength ranging from 460 to 660 nm. In addition, the produced achromatic waveplate exhibits good optical homogeneity, flexibility and can be tailored into arbitrary shapes conveniently.

Structure and design

A proper combination of multiple layers of CNC birefringent films can serve as an achromatic waveplate (Pancharatnam 1955). As a demonstration, we fabricated a 1/4 λ achromatic waveplate for the wavelength ranging from 460 to 660 nm. We adopted a three-layer structure to achieve achromatism. In a Cartesian system Oξηz illustrated in Fig. 1a, the first CNC film and the third CNC film have the same thickness $d_1 = d_3$ and the same direction of slow axis ($n_1 \parallel n_3 \parallel$ ξ-axis), while the second CNC film has a different thickness d_2 and the angle between n_1 (or ξ-axis) and the direction of slow axis n_2 of the second CNC film is denoted as θ_2. It is shown in the supporting information that the three-layer structure is equivalent to a single linear retarder with phase retardation δ and slow axis n that is at angle θ with ξ-axis. And δ and θ satisfy

$$\cos\frac{\delta}{2} = \cos\delta_1\cos\frac{\delta_2}{2} - \sin\delta_1\sin\frac{\delta_2}{2}\cos 2\theta_2 \tag{1}$$

$$\cot 2\theta = \frac{1}{\sin 2\theta_2}\left(\sin\delta_1\cot\frac{\delta_2}{2} + \cos\delta_1\cos 2\theta_2\right) \tag{2}$$

where $\delta_m = 2\pi\Delta n d_m/\lambda$ is the phase retardation of the mth (m = 1,2) CNC film, Δn is the birefringence of CNC films, λ is the wavelength of the incident light. δ and θ are generally functions of the wavelength. Compared with one-layer waveplate, the three-layer waveplate have more parameters such as δ_1, δ_2, and θ_2, which can be manipulated to achieve achromatism. In order to achieve achromatism in the range between two arbitrary wavelengths λ' and λ'' ($\lambda' < \lambda''$), we start with a tentative solution which satisfies that

$$\delta(\lambda') = \delta(\lambda'') = \Delta \tag{3}$$

$$\theta(\lambda') = \theta(\lambda'') \tag{4}$$

where Δ is the required retardation of the achromatic waveplate. Substituting Eqs. (3) and (4) into Eqs. (1) and (2) gives

$$\begin{aligned}&\cos\delta_1(\lambda')\cos\frac{\delta_2(\lambda')}{2} - \sin\delta_1(\lambda')\sin\frac{\delta_2(\lambda')}{2}\cos 2\theta_2\\ &= \cos\delta_1(\lambda'')\cos\frac{\delta_2(\lambda'')}{2}\\ &\quad - \sin\delta_1(\lambda'')\sin\frac{\delta_2(\lambda'')}{2}\cos 2\theta_2\end{aligned} \tag{5}$$

$$\begin{aligned}&\sin\delta_1(\lambda')\cot\frac{\delta_2(\lambda')}{2} + \cos\delta_1(\lambda')\cos 2\theta_2\\ &= \sin\delta_1(\lambda'')\cot\frac{\delta_2(\lambda'')}{2} + \cos\delta_1(\lambda'')\cos 2\theta_2\end{aligned} \tag{6}$$

If we introduce a "mean" wavelength $\bar{\lambda}$ which satisfies $2\Delta n(\bar{\lambda})/\bar{\lambda} = \Delta n(\lambda')/\lambda' + \Delta n(\lambda'')/\lambda''$ and a dimensionless parameter $f = \frac{\bar{\lambda}}{2\Delta n(\bar{\lambda})}[\Delta n(\lambda')/\lambda' - n(\lambda'')/\lambda'']$, then $\delta_m(\lambda') = (1+f)\delta_m(\bar{\lambda})$ and $\delta_m(\lambda'') = (1-f)\delta_m(\bar{\lambda})$. Substituting them into Eqs. (5) and (6) yields

$$\begin{aligned}&[1 - \cos\delta_1(\lambda')\cos\delta_1(\lambda'')]\cos\frac{\delta_2(\bar{\lambda})}{2}\cos\frac{f\delta_2(\bar{\lambda})}{2}\\ &= \frac{\sin\delta_1(\lambda')\sin\delta_1(\lambda'')\sin\delta_2(\bar{\lambda})}{\cos f\delta_2(\bar{\lambda}) - \cos 2\delta_2(\bar{\lambda})}\end{aligned} \tag{7}$$

$$2\cos\frac{\Delta}{2}\cos\delta_1(\bar{\lambda})\sin f\delta_1(\bar{\lambda}) = \sin\frac{f\pi}{2}\sin 2\delta_1(\bar{\lambda}) \tag{8}$$

Equation (7) and (8) are simultaneously satisfied when

$$\delta_2(\bar{\lambda}) = \pi \tag{9}$$

$$\sin f\delta_1(\bar{\lambda}) = \frac{\sin\frac{f\pi}{2}\sin\delta_1(\bar{\lambda})}{\cos\frac{\Delta}{2}} \tag{10}$$

Under this condition, θ_2 is calculated as

$$\cos 2\theta_2 = \frac{-\tan f\frac{\pi}{2}}{\tan f\delta_1(\bar{\lambda})} \tag{11}$$

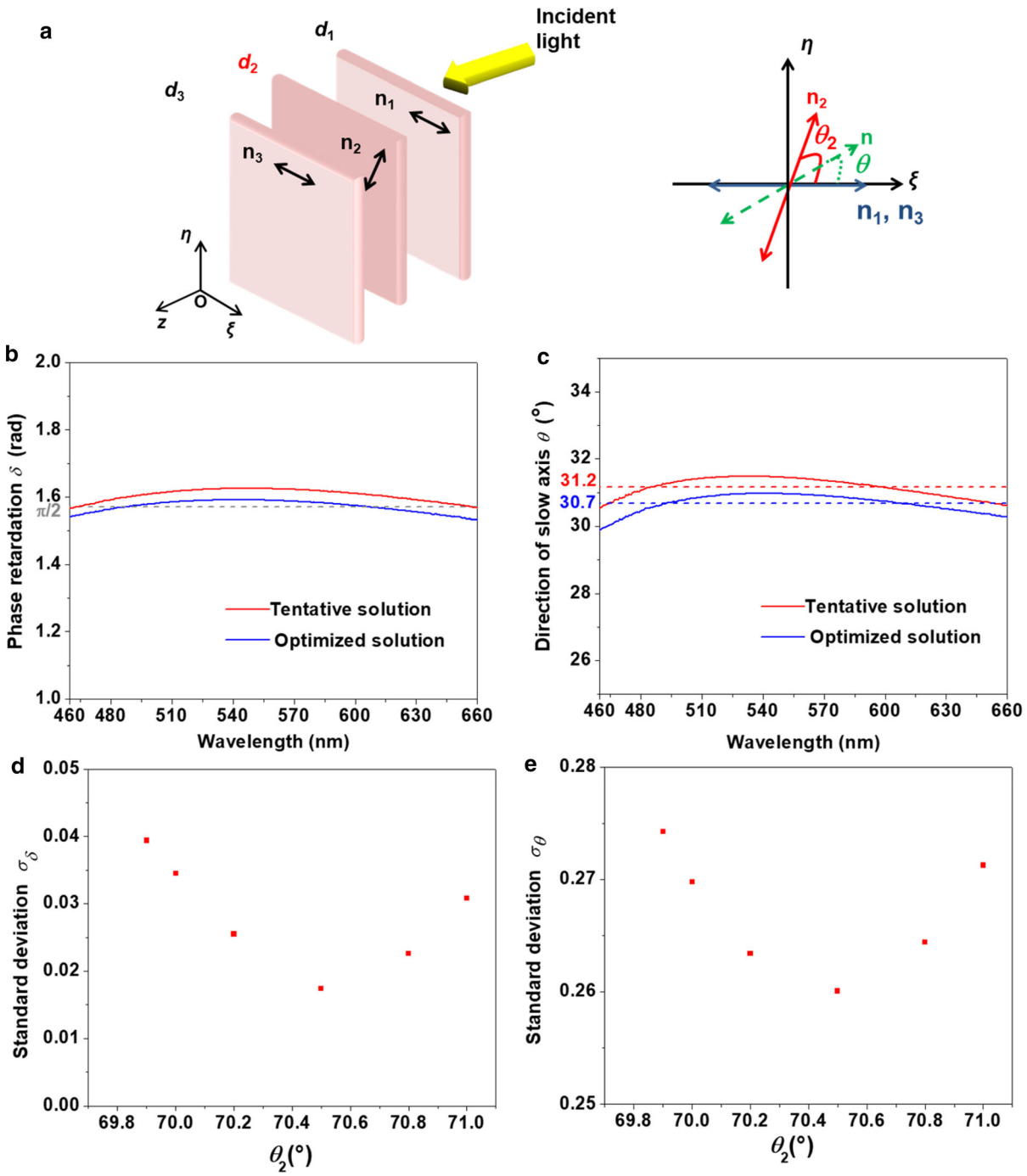

Fig. 1 **a** Schematics for the 1/4 λ achromatic CNC-based waveplate consisting of three layers of birefringent CNC films, whose slow axes are labeled as n_m and thickness is labeled as d_m (m = 1,2,3) The slow axis n of the equivalent achromatic waveplate is labeled as dashed line. **b** The calculated phase retardation $\delta(\lambda)$, and **c** the direction of slow axis $\theta(\lambda)$ of the achromatic waveplate. The red line represents the tentative solution and the blue line represents the optimized solution. The dashed line in **b** corresponds to $\delta = \pi/2$; and the dashed lines in **c** corresponds to $\theta = 30.7°$ (blue line) and $\theta = 31.2°$ (red line) respectively. The standard deviations σ_δ (for the phase retardation) **d** and σ_θ (for the direction of slow axis) **e** for solutions with different values of θ_2

In summary, in order to get the tentative solution of an achromatic CNC-based waveplate with phase retardation Δ for wavelengths ranging from λ' to λ'', first calculate the "mean" wavelength $\bar{\lambda}$ and parameter f, next determine the thickness of the second CNC film so that $\delta_2(\bar{\lambda}) = \pi$, then calculate $\delta_1(\bar{\lambda})$ by solving the Eq. (10) and determine the thickness of the first and the third CNC films, finally calculate the angle θ_2 by Eq. (11). To design a 1/4 λ achromatic waveplate ($\Delta = \pi/2$) for the wavelength $460\,\text{nm} = \lambda' \leq \lambda \leq \lambda'' = 660\,\text{nm}$, we calculate that for the tentative solution $\bar{\lambda} = 542$ nm,$f = 0.18$,$\delta_1(\bar{\lambda}) = 2.02$, $\delta_2(\bar{\lambda}) = 3.14$, $\theta_2 = 69.9°$, $d_1 = d_3 = \delta_1(\bar{\lambda})\bar{\lambda}/2\pi\Delta n(\bar{\lambda}) = 2.8\mu$m, and $d_2 = \delta_2(\bar{\lambda})\bar{\lambda}/2\pi\Delta n(\bar{\lambda}) = 4.4$ μm, where the birefringence Δn of our CNC films is measured to be $\Delta n(542\text{ nm}) \approx 0.061$ (see Characterization of single birefringent film). After substituting the values of d_1, d_2, d_3 and the birefringence $\Delta n(\lambda)$ into Eqs. (1) and (2), the phase retardation and the direction of slow axis of the achromatic CNC-based waveplate are calculated and shown in.

Figure 1b, c (red lines) respectively. For this tentative solution, the achromatism condition is met precisely at $\lambda' = 460$ nm and $\lambda'' = 660$ nm, however $\delta(\lambda)$ and $\theta(\lambda)$ deviate from their expected values for 460 nm $< \lambda <$ 660 nm. The values of $\delta_1(\bar{\lambda})$, $\delta_2(\bar{\lambda})$, and θ_2 can be optimized in the vicinity of the tentative solution so as to reduce the standard deviations $\sigma_\delta = \sqrt{\frac{1}{N}\sum_i^N \left\{\delta_i(\lambda) - \pi/2)^2\right\}}$ and $\sigma_\theta = \sqrt{\frac{1}{N}\sum_i^N \left\{\theta_i(\lambda) - \overline{\theta})^2\right\}}$ of $\delta(\lambda)$ and $\theta(\lambda)$ respectively. We fixed the value of $\delta_1(\bar{\lambda}) = 2.02$ and $\delta_2(\bar{\lambda}) = 3.14$ and only change the value of θ_2, because θ_2 has a bigger influence on σ_δ and σ_θ. The standard deviations σ_δ and σ_θ corresponding to different θ_2 are shown in Fig. 1d, e, and we finally adopt $\theta_2 = 70.5°$ that corresponds to the minimums of both σ_δ and σ_θ.

Fabrication

The rod-shaped CNCs (Fig. 2a) used in our experiment are prepared by the well-established method of acid hydrolysis of cotton (Li et al. 2019b), and CNC suspension with 13wt% of CNCs exhibiting helical alignment (pH = 2) is obtained (Fig. 2b). Adding 2 μL of 65wt% sulfuric acid to 200 μL of the CNC suspension reduces the pH to ~ 1.5 and results in uniaxial alignment of CNC LCs (Fig. 2c). The pH value is measured by a pH meter (PH5S) with 0.01 resolution. In order to improve mechanical properties of the CNC film dried from the CNC suspension, 10wt% of PEG (number-average molecular weight 400 g/mol, Sigma-Aldrich) is added to the CNC nematic LCs and the mixture remains in the nematic phase. Uniform CNC birefringent films with controllable thickness are made by aligning PEG-doped CNC nematic LCs via shearing on patterned PDMS substrates (Fig. 2d). The PDMS substrate has a pattern of gratings with a period of 800 μm, which is made by curing PDMS prepolymer on a SU-8 (photoresist) mold with the grating pattern. The dimension of the SU-8 mold is around 1.5 cm × 1.5 cm, and it is fabricated by UV-lithography (see supporting information). In order to increase the hydrophilicity, the surface of the PDMS substrates is modified by plasma treatment. The PEG-doped CNC nematic LCs is dropped on the PDMS substrate and aligned by shearing the LC with a piece of glass sliding along the ridges of the gratings. Excess CNC suspension on the ridges was removed. Therefore the height of the grating ridges of the PDMS substrate, which is determined by the height of the grating ridges of the SU-8 mold, corresponds to the thickness of the CNC LC film. Since the height of the grating ridges of the SU-8 mold can be conveniently controlled by the spin coating speed of SU-8, the thickness of the CNC LC film is well controlled. Two identical films with CNC LCs on PDMS substrate are aligned face-to-face with half-period displacement and bonded firmly to form one CNC birefringent film after the CNC suspension is completely dried at room temperature. CNCs are effectively aligned on large scale (Fig. S1. in supporting information). The striped structure of the PDMS substrate only produces slight scattering in the waveplates and doesn't change the orientation of CNCs obviously, because the period of the striped structure is large. Three CNC birefringent films with thickness $d_1 = 2.8\mu$m,$d_2 = 4.4$ μm and $d_3 = 2.8$ μm are arranged according to the design shown in Fig. 1a and bonded together by plasma treatment for 20 min. Ideally, the direction of slow axis of each CNC birefringent film is parallel to the direction of shearing, however it has to be determined with higher precision by measuring the transmission spectra of the CNC films between two polarizers. As a result, the slow

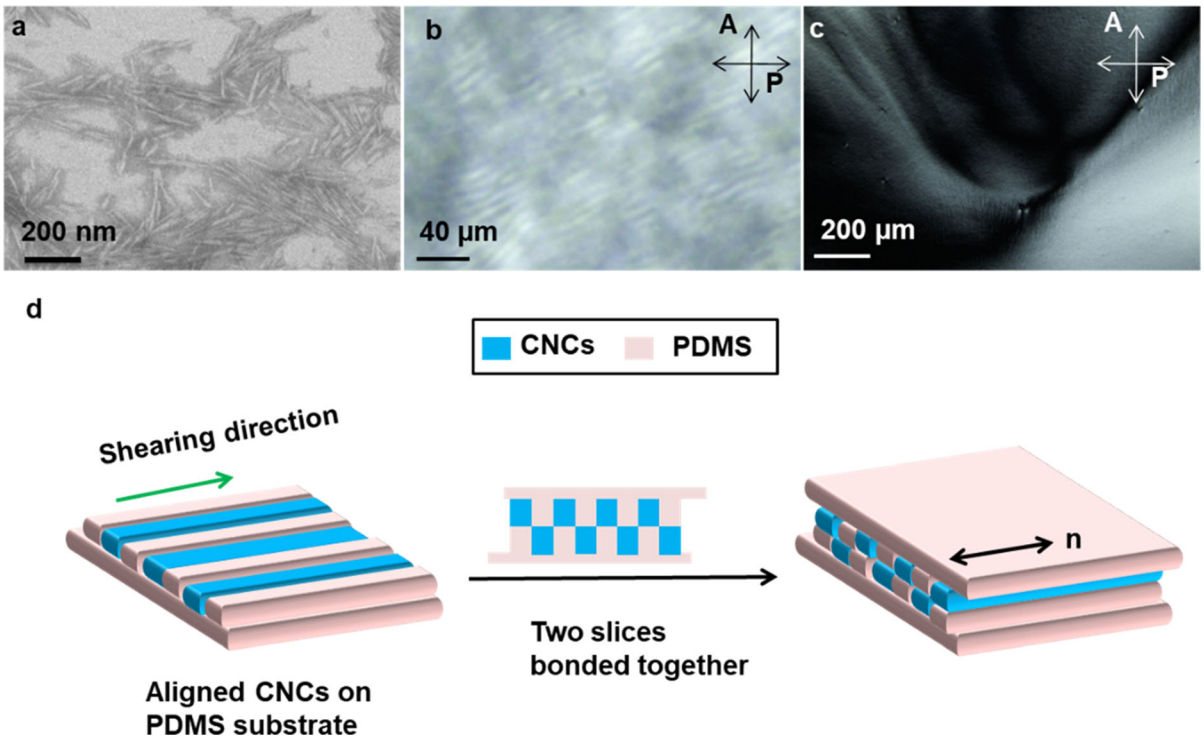

Fig. 2 **a** TEM image of the produced CNCs. Polarized optical microscopy images of **b** the helical alignment of CNC LCs with pH = 2, and **c** the uniaxial alignment of CNC LCs with pH ~ 1.5. P and A indicate the polarizations of the polarizer and the analyzer, respectively. **d** The fabrication process of the CNC birefringent film

axes of the first and the third birefringent films can be made parallel, and θ_2 can be well controlled ($\theta_2 = 70.5°$).

Characterization

Characterization of single birefringent film

The phase retardation $\delta_m(\lambda)$ and the direction of slow axis n_m of the m^{th} birefringent film are characterized by measuring the transmission spectra between two polarizers. The birefringence $\Delta n(\lambda)$ of the CNC film is extracted from the experimental result.

Figure 3a demonstrates the experimental setup for measuring the spectra of a single birefringent film. Linearly polarized incident light with the intensity I_0, which is generated by a polarizer, is focused by a condenser on the CNC film. Then the transmitted light is collected by an objective and passes through an analyzer, and finally is detected by a spectrometer. The polarization P of the polarizer is parallel with x-axis, the angle between n_m and P is denoted as θ_m, and the angle between the polarization of the analyzer and P is denoted as β. The intensity $I_m(\beta,\gamma_m)$ of the light collected by the spectrometer is

$$I_m(\beta,\gamma_m) = \frac{I_0(1-R)\,e^{-\alpha d_m}}{2}\{1+\cos 2\beta(\cos^2 2\gamma_m + \cos\delta_m \sin^2 2\gamma_m) - \sin 2\beta[(1-\cos\delta_m)\sin 2\gamma_m \cos 2\gamma_m]\} \quad (12)$$

where the reflectance $R \sim 8\%$ and the extinction $\alpha \sim 0.03\mu m^{-1}$ of the CNC films are measured to be polarization and wavelength insensitive (see supporting information), and the PDMS substrate exhibits negligible birefringence. When β is fixed at $\beta = 90°$ and the CNC film is rotated, the intensity $I_m(90°,\gamma_m)$ is maximized when $\gamma_m = 45°$ or $\gamma_m = 135°$. This allows high-precision determination of the direction of slow axis of the CNC film. Inserting a 530 nm λ-plate with

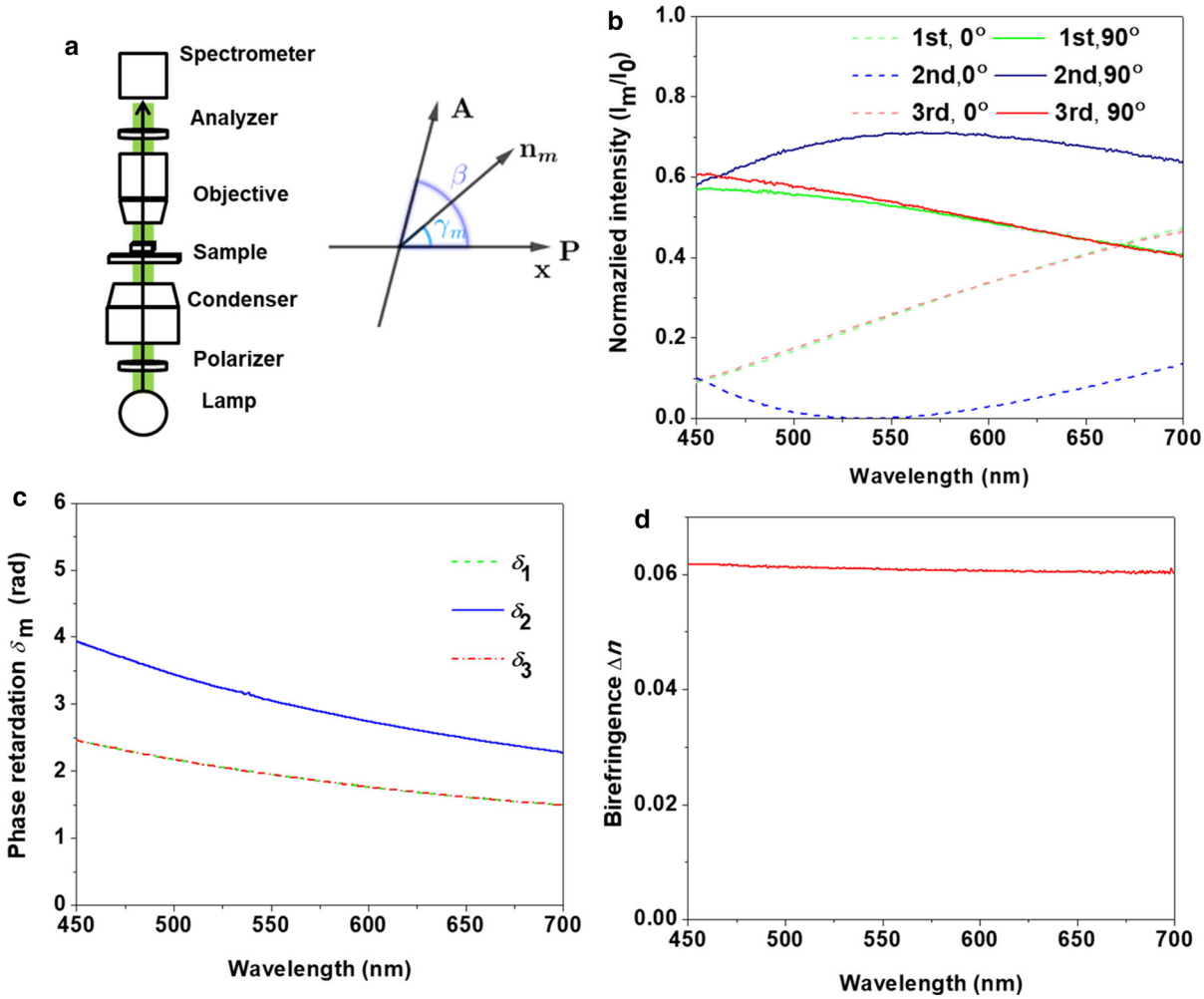

Fig. 3 **a** The experimental setup for measuring transmission spectra for CNC birefringent films. **b** When the slow axis of the CNC film is at 45° with the polarization of the polarizer ($\gamma_m = 45°$), the measured transmission spectra $I_m(\beta,45°)/I_0$ of the mth CNC birefringent film with the polarization of the analyzer parallel ($\beta = 0°$) or orthogonal ($\beta = 90°$) to the polarization of the polarizer. **c** The calculated phase retardation $\delta_m(\lambda)$ of the mth CNC birefringent film. **d** The calculated birefringence $\Delta n(\lambda)$ of the CNC film extracted from $I_3(0°,45°)/I_0$

its slow axis at 45° with x-axis after the CNC film allows us to differentiate between the fast and slow axes (Linge Johnsen et al. 2018). Then we measure the phase retardation of the CNC film. When γ_m is fixed at $\gamma_m = 45°$,

$$I_m(\beta, 45°) = \frac{I_0(1-R)e^{-\alpha d_m}}{2}(1 + \cos 2\beta \cos \delta_m) \tag{13}$$

By rotating the analyzer and measuring the transmission spectra with $\beta = 0°$ and $\beta = 90°$, the phase retardation δ_m of the CNC film can be calculated as

$$\delta_m = \cos^{-1}\left[\frac{I_m(0°,45°) - I_m(90°,45°)}{I_m(0°,45°) + I_m(90°,45°)}\right] \tag{14}$$

During the experiment, we found that even though the thickness of the CNC film may vary after drying, the phase retardation of the CNC film remained unchanged. Therefore, it's sufficient to control the phase retardation of the CNC film by controlling its thickness before its drying. Furthermore the birefringence of the CNC film can be expressed as

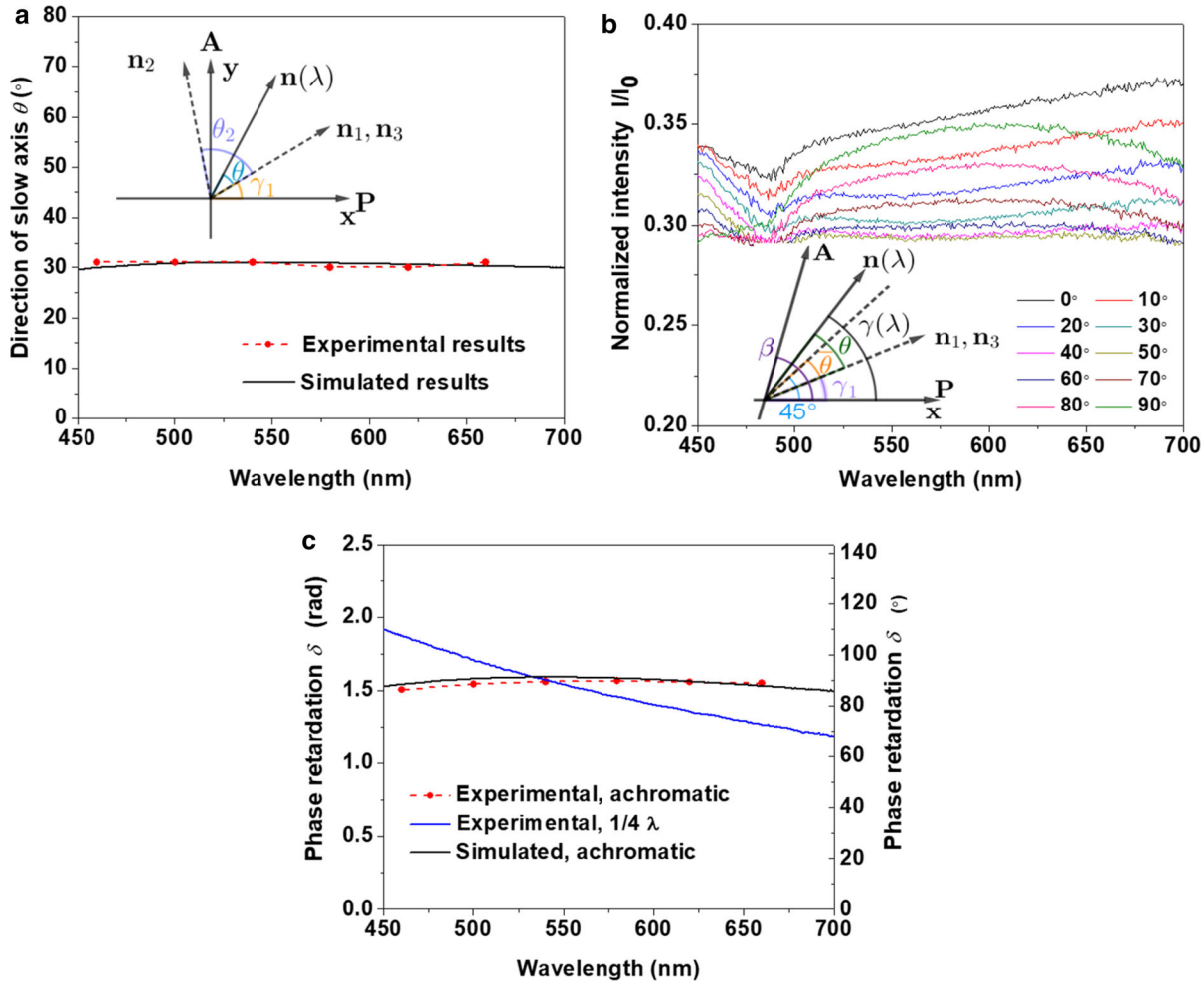

Fig. 4 **a** The experimental (red line) and simulated (black line) results for the direction of slow axis of the achromatic CNC-based waveplate. **b** The measured transmission spectra $I(\beta,\gamma)/I_0$ ($\gamma(\lambda) = 45° + \theta(\lambda) - \bar{\theta}$) of the achromatic CNC -based waveplate with different β. **c** The experimental (red line) and simulated (black line) results for the phase retardation of the achromatic CNC-based waveplate. The phase retardation of a 1/4λ waveplate (for $\bar{\lambda} = 542$ nm) consisting of only one layer of CNC film is depicted (blue line) as comparison

$$\Delta n(\lambda) = \frac{\lambda}{2\pi d_m}\cos^{-1}\left[\left(\frac{2I_m(\beta,45°)}{(1-R)e^{-\alpha d}I_0} - 1\right)\Big/\cos 2\beta\right] \quad (15)$$

Figure 3b exhibits the measured transmission spectra $I_m(\beta,45°)/I_0$ of the three CNC films and their phase retardations are calculated and shown in Fig. 3c. At $\bar{\lambda} = 542$ nm, the phase retardations $\delta_1(542\text{ nm}) = \delta_3(542\text{ nm}) = 1.99$ and $\delta_2(542\text{ nm}) = 3.12$ follow our design. Figure 3d presents the calculated birefringence of CNC films based on the curve $I_3(0°,45°)/I_0$.

Characterization of the CNC-based achromatic waveplate

The direction of slow axis $n(\lambda)$ and the phase retardation $\delta(\lambda)$ of the CNC-based achromatic waveplate are characterized using the experimental setup shown in Fig. 3a. Still we use γ_1 ($\gamma_1 \in [0, 180°)$) to denote the angle between P and n_1 (Fig. 4a). When measuring the orientation of $n(\lambda)$, β is fixed at $\beta = 90°$ (crossed polarizers), and the achromatic waveplate is rotated. When $\gamma_1 = \gamma_{1\max}(\lambda) \in (0, 90°)$, the intensity $I(\lambda,\gamma_1)$ at wavelength λ reaches its maximum with $\gamma_{1\max}(\lambda) + \theta(\lambda) = 45°$, so that $\theta(\lambda)$ is calculated as

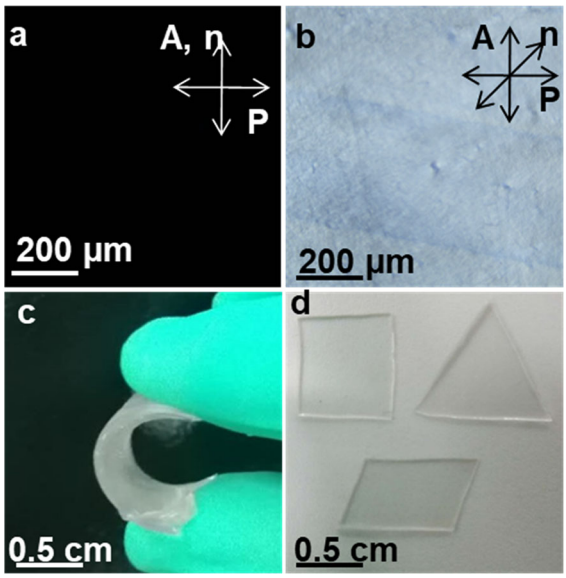

Fig. 5 Polarized optical microscopy images of the 1/4λ achromatic CNC-based waveplate with **a** $n(\bar{\lambda})$ perpendicular to P, and **b** $\mathbf{n}(\bar{\lambda})$ orientated 45° with respect to P. P and A represent the polarizations of the polarizer and the analyzer, respectively. The flexible 1/4λ achromatic CNC-based waveplate can be bent easily **c** and can be tailored into square, triangle and parallelogram shapes conveniently **d**

$\theta(\lambda) = 45° - \gamma_{1\,\max}(\lambda)$ and shown in Fig. 4a. The average value $\bar{\theta}$ of $\theta(\lambda)$ is estimated to be $\bar{\theta} \approx 30.7°$, and the maximum deviation $(\Delta\theta)_m$ of $\theta(\lambda)$ is estimated to be $(\Delta\theta)_m = \max\{|\theta(\lambda) - \bar{\theta}|\} \approx 0.6°$. Our results show that all the wavelengths between 460 and 660 nm have similar slow axis as expected. We then measure the phase retardation $\delta(\lambda)$ of the CNC-based achromatic waveplate. The orientation of the achromatic retarder is fixed at $\gamma_1 = $ '14.3° so that $\gamma_1 + \bar{\theta} = 45°$, then the angle γ between $\mathbf{n}(\lambda)$ and P satisfies $\gamma(\lambda) = 45° + \theta(\lambda) - \bar{\theta}$(Fig. 4b, inset). When the analyzer is rotated, the intensity $I(\beta,\gamma)$ of the light collected by the spectrometer is

$$I(\beta,\gamma) = \frac{I_0(1-R)\,e^{-\alpha\sum d_m}}{2}\{1 + \cos 2\beta(\cos^2 2\gamma + \cos\delta \sin^2 2\gamma) - \sin 2\beta[(1 - \cos\delta)\sin 2\gamma \cos 2\gamma]\} \tag{16}$$

Therefore the phase retardation δ is calculated as

$$\cos\delta = \frac{1}{\sin^2 2\gamma}\left[\frac{I(0°,\gamma) - I(90°,\gamma)}{I(0°,\gamma) + I(90°,\gamma)} - \cos^2 2\gamma\right] \tag{17}$$

Figure 4b demonstrates the measured transmission spectra $I(\beta,\gamma)$ of the achromatic waveplate, and its phase retardation δ is calculated and shown in Fig. 4c. For the wavelengths ranging from 460 to 660 nm, δ is measured to be around $\pi/2$ which agrees with the simulated results (Fig. 4c, black line). The maximum deviation $(\Delta\delta)_m$ of $\delta(\lambda)$ is estimated to be $(\Delta\delta)_m = \max\{|\delta(\lambda) - \pi/2|\} \approx 0.06$. As a comparison, we also fabricate a 1/4λ waveplate for $\bar{\lambda} = 542$ nm, which consists of only one layer of CNC film. Its phase retardation is measured (blue line in Fig. 4c) and shows a maximum deviation ~ 0.5. Our design improves the achromatism of the optical waveplate by about one order of magnitude.

The polarizing optical microscopy images of the achromatic waveplate can be obtained by replacing the spectrometer in Fig. 3a with a CCD ($\beta = 90°$ is fixed). When the achromatic waveplate is rotated so that $\gamma \approx 90° - \bar{\theta} = 59.3°$ or $\gamma \approx 180° - \bar{\theta} = 149.3°$, all light should be blocked (Fig. 5a). When $\gamma \approx 45° - \bar{\theta} = 14.3°$ or $\gamma \approx 135° - \bar{\theta} = 104.3°$, the imaged areas are the brightest (Fig. 5b). The uniform texture shown in the microscopic images (Fig. 5a, b) reveals that the CNC nematic LCs are uniformly aligned and the achromatic waveplate exhibits good optical homogeneity. In addition, the produced achromatic waveplate is flexible and can be bent or tailored into any arbitrary shape easily (Fig. 5c, d).

Conclusions

In conclusion, we have proposed and fabricated a 1/4 λ achromatic CNC-based waveplate composed of three layers of birefringent CNC films, whose phase retardation and slow axis direction are calculated by the Jones matrix, and achromatic properties are also optimized with the smallest standard deviations. Each CNC film with desired phase retardation is produced by aligning CNC nematic LCs doped with polyethylene glycol on patterned PDMS substrates. The obtained CNC-based achromatic waveplate is characterized by measuring the transmission spectra of the waveplate between two polarizers, and presents a

maximum deviation of phase retardation of 0.06 for the wavelength ranging from 460 to 660 nm. Low cost, flexible and achromatic 1/4λ waveplates from the renewable CNCs may find a potential application in advanced optical materials and devices.

Funding The work was supported by National Natural Science Foundation of China (12004332, 61850410525, 61550110246), Postdoctoral Science Foundation of China (2019M662018), and Key Research and Development Program of Zhejiang Province (2021C03178).

Declarations

Conflict of interest The authors claim no conflicts of interests.

References

Abuleil MJ, Abdulhalim I (2014) Tunable achromatic liquid crystal waveplates. Opt Lett 39:5487–5490

Araki J, Kuga S (2001) Effect of trace electrolyte on liquid crystal type of cellulose microcrystals. Langmuir 17:4493–4496

Beck S, Bouchard J, Chauve G, Berry R (2013) Controlled production of patterns in iridescent solid films of cellulose nanocrystals. Cellulose 20:1401–1411

Beckers JM (1971) Achromatic linear retarders. Appl Opt 10:973–975

Chen L, Wang Q, Hirth K, Baez C, Agarwal UP, Zhu JY (2015) Tailoring the yield and characteristics of wood cellulose nanocrystals (CNC) using concentrated acid hydrolysis. Cellulose 22:1753–1762

Cranston ED, Gray DG (2008) Birefringence in spin-coated films containing cellulose nanocrystals. Coll Surf, A 325:44–51

De La Cruz JA, Liu Q, Senyuk B, Frazier AW, Peddireddy K, Smalyukh II (2018) Cellulose-based reflective liquid crystal films as optical filters and solar gain regulators. ACS Photon 5:2468–2477

Fernandes SN, Almeida PL, Monge N, Aguirre LE, Reis D, de Oliveira CLP, Neto AMF, Pieranski P, Godinho MH (2017) Mind the microgap in iridescent cellulose nanocrystal films. Adv Mater 29:1603560

Frka-Petesic B, Vignolini S (2019) So much more than paper. Nat Photon 13:365–367

Habibi Y, Lucia LA, Rojas OJ (2010) Cellulose nanocrystals: chemistry, self-assembly, and applications. Chem Rev 110:3479–3500

Hariharan P (1995) Achromatic retarders using quartz and mica. Meas Sci Technol 6:1078–1079

Hariharan P (2002) Broad-band apochromatic retarders: choice of materials. Opt Laser Technol 34:509–511

Haywood AD, Haywood AD, Davis VA, Davis VA (2017) Effects of liquid crystalline and shear alignment on the optical properties of cellulose nanocrystal films. Cellulose 24:705–716

Hoeger I, Rojas OJ, Efimenko K, Velev OD, Kelley SS (2011) Ultrathin film coatings of aligned cellulose nanocrystals from a convective-shear assembly system and their surface mechanical properties. Soft Matter 7:1957–1967

Jen Y-J, Lakhtakia A, Yu C-W, Lin C-F, Lin M-J, Wang S-H, Lai J-R (2011) Biologically inspired achromatic waveplates for visible light. Nat Commun 2:363

Jonoobi M, Oladi R, Davoudpour Y, Oksman K, Dufresne A, Hamzeh Y, Davoodi R (2015) Different preparation methods and properties of nanostructured cellulose from various natural resources and residues: a review. Cellulose 22:935–969

Kose O, Tran A, Lewis L, Hamad WY, MacLachlan MJ (2019) Unwinding a spiral of cellulose nanocrystals for stimuli-responsive stretchable optics. Nat Commun. https://doi.org/10.1038/s41467-019-08351-6

Lagerwall JPF, Schütz C, Salajkova M, Noh J, Hyun Park J, Scalia G, Bergström L (2014) Cellulose nanocrystal-based materials: from liquid crystal self-assembly and glass formation to multifunctional thin films. NPG Asia Mater 6:e80–e80

Li C, Wang N, Guo T, Evans J, He S (2019a) Preparation of optical waveplates from cellulose nanocrystal nematics on patterned polydimethylsiloxane substrates. Opt Mater Exp 9:4614–4623

Li CX, Evans J, Wang N, Guo TB, He SL (2019b) pH dependence of the chirality of nematic cellulose nanocrystals. Sci Rep 9:11290–11297

Ling Z, Edwards JV, Guo Z, Prevost NT, Nam S, Wu Q, French AD, Xu F (2019) Structural variations of cotton cellulose nanocrystals from deep eutectic solvent treatment: micro and nano scale. Cellulose 26:861–876

Linge Johnsen SA, Bollmann J, Lee HW, Zhou Y (2018) Accurate representation of interference colours (Michel–Lévy chart): from rendering to image colour correction. J Microsc 269:321–337

Mendoza-Galván A, Tejeda-Galán T, Domínguez-Gómez AB, Mauricio-Sánchez RA, Järrendahl K, Arwin H (2019) Linear birefringent films of cellulose nanocrystals produced by dip-coating. Nanomaterials 9:45

Pan J, Hamad W, Straus SK (2010) Parameters affecting the chiral nematic phase of nanocrystalline cellulose films. Macromolecules 43:3851–3858

Pancharatnam S (1955) Achromatic combinations of birefringent plates: part II. An achromatic quarter-wave plate. Proce Indian Acad Sci—Sect A 41:137–144

Parker RM, Guidetti G, Williams CA, Zhao T, Narkevicius A, Vignolini S, Frka-Petesic B (2018) The self-assembly of cellulose nanocrystals: hierarchical design of visual appearance. Adv Mater 30:1704477-n/a

Qu D, Zheng H, Jiang H, Xu Y, Tang Z (2019) Chiral photonic cellulose films enabling mechano/chemo responsive selective reflection of circularly polarized light. Adv Opt Mater 7:1801395

Roberts NW, Chiou TH, Marshall NJ, Cronin TW (2009) A biological quarter-wave retarder with excellent achromaticity in the visible wavelength region. Nat Photon 3:641–644

Saha A, Bhattacharya K, Chakraborty AK (2012) Achromatic quarter-wave plate using crystalline quartz. Appl Opt 51:1976–1980

Sun B, Zhang M, Hou Q, Liu R, Wu T, Si C (2016) Further characterization of cellulose nanocrystal (CNC) preparation from sulfuric acid hydrolysis of cotton fibers. Cellulose 23:439–450

Tran A, Boott CE, MacLachlan MJ (2020) Understanding the self-assembly of cellulose nanocrystals—toward chiral photonic materials. Adv Mater 32:1905876

Yao K, Meng Q, Bulone V, Zhou Q (2017) Flexible and responsive chiral nematic cellulose nanocrystal/poly(-ethylene glycol) composite films with uniform and tunable structural color. Adv Mater 29:1701323-n/a

Yu HY, Qin ZY, Lin L, Yang XG, Zhou Y, Yao JM (2013) Comparison of the reinforcing effects for cellulose nanocrystals obtained by sulfuric and hydrochloric acid hydrolysis on the mechanical and thermal properties of bacterial polyester. Compos Sci Technol 87:22–28

Zhao TH, Parker RM, Williams CA, Lim KTP, Frka-Petesic B, Vignolini S (2018) Printing of responsive photonic cellulose nanocrystal microfilm arrays. Adv Funct Mater 29:1804531-n/a